Journal of Russian Laser Research, Volume 34, Number 5, September, 2013

HEATING OF LOW-DENSITY MATTER BY SOFT X-RAY RADIATION AND RADIATION WAVES

G. A. Vergunova,[1]* V. B. Rozanov,[1] A. S. Grushin,[2] V. G. Novikov,[2] N. Yu. Orlov,[3] and O. N. Rozmej[4]

[1] *P. N. Lebedev Physical Institute, Russian Academy of Sciences*
Leninskii Prospect 53, Moscow 119991, Russia

[2] *M. V. Keldysh Institute of Applied Mathematics, Russian Academy of Sciences*
Miusskaya Square 4, Moscow 125047, Russia

[3] *Joint Institute for High Temperatures, Russian Academy of Sciences*
Izhorskaya Street 13, Bd. 2, Moscow 125412, Russia

[4] *GSI Helmholtzzentrum für Schwerionenforschung GmbH*
Planckstrasse 1, Darmstadt 164291, Germany

*Corresponding author e-mail: verg@sci.lebedev.ru

Abstract

We investigate the nonlinear radiative thermal conductivity model, which is theoretically well substantiated and based on a small number of assumptions. We consider the spatial and temporal evolutions for a low-density polymer foam heated by radiation waves taking into account the dependence of the absorption coefficients on the quantum energy. The form of the radiation wavefront (its slope and speed of propagation) differs from the classical form by a low-temperature "tongue" penetrating deep into the plasma. The plasma in this segment of the wavefront is heated up to a temperature of 1–2 eV by photons in the hard part of the spectrum, with energies for which $h\nu/kT > 4$. We simulate numerically the experiments at the PHELIX facility to heat a low-density cellulose triacetate (TAC, $C_{12}H_{16}O_8$) taking into account the radiation transfer. The energy and the spectral flux of radiation that passed through the TAC layer are satisfactorily consistent with the experimental results.

Keywords: laser plasma, radiation interaction with matter, radiation heat waves, radiation spectral flux.

1. Introduction

Radiative thermal conductivity or radiation waves play an important role in the energy transfer in laser plasmas, Z-pinches, thermonuclear fusion targets, and astrophysics. Propagation of nonlinear radiation waves in matter has been well studied theoretically [1–4]. For a radiation wave to exist, the size of the system should exceed several times the photon free path length typical for this medium, i.e., the medium should be optically nontransparent. In addition, the energy of heating an external source should be consistent with the size of the heated system. In this case, hard photons heat the plasma layers, whose thickness is close to the free path length, and the heated layers will themselves become radiation

Translated from manuscript submitted on April 15, 2013.
1071-2836/13/3405-0441

sources and heat even deeper layers of the target. Herewith, the radiation intensity should be close to the equilibrium Planck intensity corresponding to the temperature in a given point, i.e., the condition of local thermodynamic equilibrium (LTE) must be fulfilled.

The propagation of radiation waves is dealt with in a large number of experimental and theoretical works. In [5–7] the propagation of radiation waves in solid material has been experimentally investigated. In [8], it was first noted that a decrease in the density at the preserved mass of the target led to increase in the energy transformed into the internal energy and then into radiation, and to the suppression of the transition into kinetic energy. In [9], the use of low-density materials with high Z, including, as additions, elements with high Z, was shown to increase radiation and contribute to a decrease of plasma losses for hydrodynamic motion.

Technologies for production of polymer materials developed in recent years have enabled fabrication of homogeneous targets from foam-like materials of preset low densities [10–12]. Additions of heavy elements to foams enable the change in the optical path lengths within broad limits to provide one with conditions required to form radiation waves. Namely, the path length should be smaller than the size of the system, and the LTE condition should be fulfilled. Such systems are used to study the classical regime of radiation waves. A comparison of experimental data with theoretical calculations can be used to verify the optical constants of the plasma.

Experimental research on the propagation of the radiation wave through low-density material has been carried out. In [13], the flux of X-ray radiation has been experimentally shown to increase with decrease in the matter density. In the experiments, a foam Ta_2O_5 with densities of 100 and 4 mg/cm^3 was used. In [14], the time for passage of the radiation wave through a plane layer of agar–agar ($C_{12}H_{18}O_9$), density 5, 10, and 20 mg/cm^3, and SiO_2 aerogel, density 50 mg/cm^3, has been measured. The transfer of radiation waves through plane targets from low-density C_6H_{12} plastic foams, as well as foams with copper additions into the plastic ($C_6H_{12}Cu_{0.394}$) of density 50 mg/cm^3, has been experimentally investigated [15].

In [16], radiation transfer has been considered in Ta_2O_5 aerogel foam of density 40 mg/cm^3 and in SiO_2 aerogel foam of density 50 mg/cm^3. Experiments with foams at the PALS facility, Prague [17,18] and the LIL facility, Bordeaux [19] have been carried out. Foam targets have also been investigated in other works with respect to various applications. In particular, there are plans to investigate ion-beam slowdown in plasma in experiments at the PHELIX facility [20, 21]. In those experiments, plasma is created as the result of indirect heating of low-density polystyrene foam of density $\rho = 0.001 - 0.01$ g/cm^3 under the action of a pulse of the X-ray radiation, into which the laser radiation is initially transformed. The action of the external X-ray radiation source on the low-density foam forms a plasma with relatively spatially homogeneous density and temperature profiles. Interaction of soft X-ray radiation with low-density matter was considered in [21, 22].

Since the matter is heated by radiation waves, we pay more attention to the description of the radiative thermal conductivity wave as to the theoretical model close to a real physical experiment. In this paper, we deal with the heating of a low-density matter by soft X-ray radiation in a concrete situation implemented in the experiment. However, this work has a more general meaning, since it analyzes the possibility of achieving conditions under which the transfer processes are performed by means of radiative thermal conductivity. At relatively low energies of the laser and small sizes of the plasma, these experiments create conditions for implementing the radiation-wave propagations, and the theoretical approach can be compared with the experimental results. Thus, there is a unique possibility to investigate the radiative thermal conductivity model, which is theoretically well substantiated and relies on a small number of assumptions. Further research in this direction is of great interest, since the theoretical model opens up

the possibility of verifying optical constants.

Experiments at the PHELIX facility [20, 21] make use of an Nd laser with energy of ∼250–300 J at the first harmonic and ∼150–180 J at the second harmonic, with pulse length of 1 ns. The laser radiation enters a gold cylinder and heats the cylinder's surface. Inside the cylinder's surface, the gold heats up and evaporates. The quanta originating in the laser-heated region leave it and are absorbed in the cold layers of the cylinder's inner surface. As the heating continues, the entire surface of the cylinder becomes a source of soft X-ray radiation. The radiation leaves the cylinder through its open butt ends. Adjacent to the cylinder's base opposite to the laser is a plane layer of foamy cellulose triacetate (TAC, $C_{12}H_{16}O_8$) of density 2–10 mg/cm^3.

At given laser energies, a flux of soft X-ray radiation with effective temperature corresponding to a blackbody temperature $T_{\rm Pl} = 20 - 40$ eV is incident on the foam target. However, the flux of external radiation exiting the gold cylinder and incident on the TAC plasma is not the Planck one corresponding to a single temperature. Moreover, it changes with time. In this sense, it is not in equilibrium. At such temperatures, there are ions with several degrees of ionization for each element in the TAC plasma. Even for light ions, calculations of the ionization composition of plasma, spectral coefficients of absorption, and Rosseland and Planck mean photon-emission path lengths are a complex and labor-intensive task. With increase in the charge of the plasma ions, the task becomes even more complicated. There are many works on the calculation of optical constants, in particular, databases [23–25].

2. Energy Transfer by Radiation under Nonlinear Thermal Conductivity Conditions

Consider the heating of a matter by means of photons. The energy transfer in the plasma by radiation with the help of nonlinear thermal conductivity is performed at radiation energy densities close to equilibrium. The thermal conductivity coefficient depends on temperature in a power-law way. In the case of weak anisotropy of the radiation field, the radiation flux W_ν at the spectral frequency ν is related to the radiation density U_ν as follows [2]:

$$W_\nu = -l'_\nu c \nabla U_\nu / 3, \tag{1}$$

where c is the speed of light, and $l'_\nu = 1/\chi'_\nu$ is the photon free path length, where induced emission at the spectral frequency ν is taken into account.

If the diffusion approximation is valid, the condition of local thermodynamic equilibrium is satisfied, and $U_\nu \approx U_{\nu p}$, where $U_{\nu p} = 8\pi h\nu^3 c^{-3} / \left(e^{h\nu/T} - 1\right)$ is the equilibrium Planck function of the radiation density at frequency ν. The equilibrium radiation density integrated with respect to quantum energies is $U_p = \int\limits_0^\infty U_{\nu p}\, d\nu = 4\sigma T^4/c$, where σ is the Boltzmann constant. If local thermodynamic equilibrium for the photon-energy spectral interval (a peculiarity of this problem) is satisfied, then, by integrating (1) with respect to all spectral frequencies, we obtain an equation describing the energy transfer with the help of radiative thermal conductivity [2]

$$W = -\frac{l_{\rm Ross} c}{3} \nabla U = -\frac{16\, \sigma T^3 l_{\rm Ross} c}{3} \frac{\partial T}{\partial x}, \tag{2}$$

where $l_{\text{Ross}} = \int_0^\infty l'_\nu \frac{dU_{\nu p}}{dT}\, d\nu \left[\int_0^\infty \frac{dU_{\nu p}}{dT}\, d\nu\right]^{-1}$ is the Rosseland mean free path, and $W = \int_0^\infty W_\nu\, d\nu$ is the total radiation flux integrated with respect to frequencies.

We assume that the matter is heated with the help of a flux of radiative thermal conductivity and has no time to get into motion, i.e., the propagation velocity of the radiation wave v_{rw} is greater than the speed of sound in the medium c_s ($v_{\text{rw}} > c_s$). Then the energy-balance equation has the form

$$\frac{\partial \varepsilon}{\partial t} = -\frac{1}{\rho}\left(\frac{\partial W}{\partial x} + p\frac{\partial}{\partial t}\frac{1}{\rho} + \frac{\partial W_e}{\partial x}\right),$$

where $\varepsilon = B^*T$ is the internal energy per mass unit, p is the plasma pressure, ρ is the plasma density, and W_e is the electron thermal conductivity flux. Assuming that the radiative thermal conductivity is the favored process, we obtain the following equation:

$$\frac{\partial \varepsilon}{\partial t} = -\frac{1}{\rho}\frac{\partial W}{\partial x}. \tag{3}$$

Table 1. Rosseland Path Lengths (in cm) Calculated [24] for TAC.

ρ, g/cm^3	$T = 20$ eV	$T = 30$ eV	$T = 40$ eV
0.001	0.191	2.39	13.9
0.002	0.0585	0.676	3.65
0.003	0.0242	0.29	1.54

Within the range of densities 1–3 mg/cm^3 and temperatures 5–40 eV, the Rosseland path length can be fitted using the formula

$$l_{\text{Ross}} = \delta\, T^m/\rho^\alpha \quad [\text{cm}]. \tag{4}$$

In view of the data of Table 1, we assume in (4) $\delta = 10^{-10}$, $m = 3.1$, and $\alpha = 1.8$ (T is in [eV] and ρ in [g/cm^3]). In the case under consideration, we assume, at the boundary, a constant flow of heat W_0 coming to the plane layer from the outside at $x = 0$. In the thermal-wave propagation domain, we determine the mean temperature, in order of magnitude, using the equation

$$W_0 = -\frac{16\,\sigma T^3 c}{3}\,\frac{\delta T^m}{\rho^\alpha}\,\frac{T}{x_{\text{rw}}}. \tag{5}$$

From the energy-conservation equation it follows that

$$\frac{B^*T}{t} \sim \frac{W_0}{\rho x_{\text{rw}}}. \tag{6}$$

In view of the two approximate equations, the radiation-wave propagation as a function of time is determined by the formula

$$x_{\text{rw}} \sim \left[\frac{16\,\sigma\delta c}{3\rho^\alpha(\rho B^*)^{m+4}}\right]^{1/(m+5)} W_0^{(m+3)/(m+5)} t^{(m+4)/(m+5)}. \tag{7}$$

In Fig. 1, we present the temporal dependence of the coordinate for the radiation-wavefront propagation through the TAC plasma for different values of the initial plasma densities equal to 1, 2, and 3 mg/cm^3 calculated using formula (7). The flux incident on the plasma $W_{\text{Pl}} = \sigma T_{\text{Pl}}^4$ corresponds to the temperature $T_{\text{Pl}} = 25$ eV and pulse duration 10 ns. In Fig. 1, we show the coordinate of the radiation wavefront propagation through a TAC plasma of density 3 mg/cm^3 for fluxes of heating radiation with Planck temperatures of 15, 20, and 25 eV. In Figs. 1–2, we also show the numerically calculated coordinate of the radiation-wave propagation through the TAC plasma. The radiation-wave-propagation velocity proved to be lower than the values obtained using formula (7).

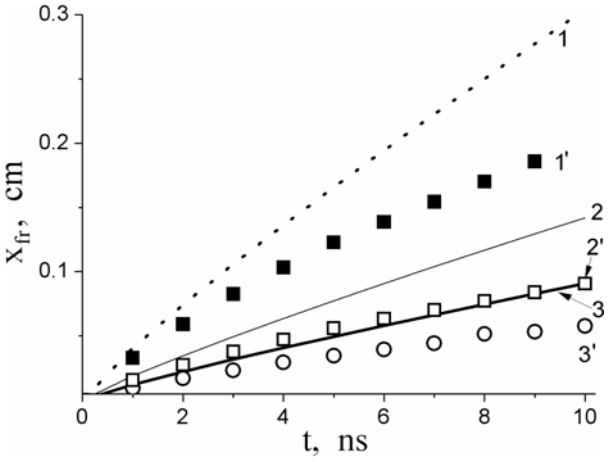

Fig. 1. Radiation front position vs time. The initial densities of the plasma are 1 mg/cm^3 (curves 1 and 1′), 2 mg/cm^3 (curves 2 and 2′), and 3 mg/cm^3 (curves 3 and 3′). Curves 1, 2, and 3 are calculated using formula (7). The results of numerical simulation are shown by curves 1′, 2′, and 3′.

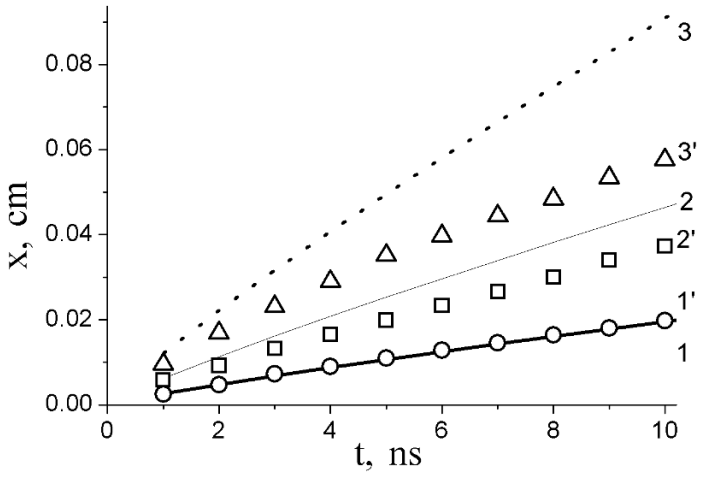

Fig. 2. Radiation front position vs time. The incident flux corresponds to the incident radiation temperature of 15 eV (curves 1 and 1′), 20 eV (curves 2 and 2′), and 25 eV (curves 3 and 3′). Curves 1, 2, and 3 are calculated using formula (7). The results of numerical modeling are shown by curves 1′, 2′, and 3′.

3. Results of Numerical Modeling

We proceed with numerical modeling of plasma formation in a plane layer of a polymer foam under the action of an external thermal flux using the one-dimensional numerical code RADIAN [22,26] which, along with two-temperature hydrodynamic equations, considers radiation transfer in a multigroup approximation. The range of spectral energies up to 400 eV was split into 130 groups. The propagation of the external heating flux of radiation and the transfer of the plasma's intrinsic radiation are taken into account. This series of calculations makes use of optical absorption coefficients calculated according to the techniques adopted from [23,24].

A series of calculations was done in which the varied parameters were the external radiation flux incident on the plasma layer $T_{\rm Pl} = 20 - 40$ eV, duration of this external pulse $\tau_{\rm Pl} = 5 - 10$ ns, thickness of the plasma layer $\Delta = 700 - 2000$ μm, and the initial density of the plasma layer ($\rho_0 = 1 - 3$ mg/cm^3). Optical constants of the plasma were also varied. At the considered parameters of the plasma and heating radiation, the speed of the radiation wave is greater than the speed of sound, and the plasma does not have time to move off position. Nevertheless, despite the leading role of the radiative thermal conductivity, the energy also gets to the medium in a hydrodynamic way, and formation of the compression and depression waves occurs, which transfers the pulse forward. The speed of the radiation wave depends on the density as $\sim \rho^{-(\alpha+m+4)/(m+5)} = \rho^{-1.1}$. With increase in density it decreases, and the role of hydrodynamic processes increases. Thus, at a flux of the plasma-heating radiation with an effective Planck temperature of 25 eV, for time 5 ns, the radiation wave in the plane case at a density of 3 mg/cm^3 will heat a 300 μm thick layer, at a density of 2 mg/cm^3 will heat a 600 μm thick layer (Fig. 1).

The evolution of the radiation-wave propagation is shown in Figs. 3–4 (the wave is incident on the left-hand side). Figure 3 presents the density and temperature profiles formed in a plane layer of the TAC plasma under the action of a Planck flux of radiation with a temperature of 25 eV and duration of 10 ns.

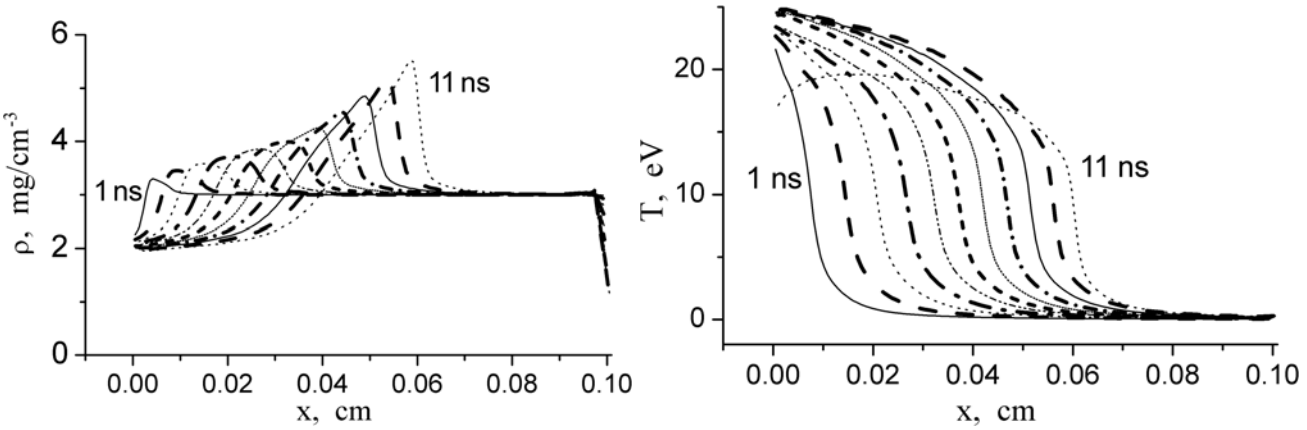

Fig. 3. The density (left) and temperature (right) profiles formed in a plane layer of plasma at time changed from 1 to 11 ns with a step of 1 ns. A homogeneous plasma layer with initial density 3 mg/cm^3 and thickness 1000 μm was irradiated by a thermal source with Planck radiation temperature 25 eV for 10 ns from the left boundary at $x = 0$.

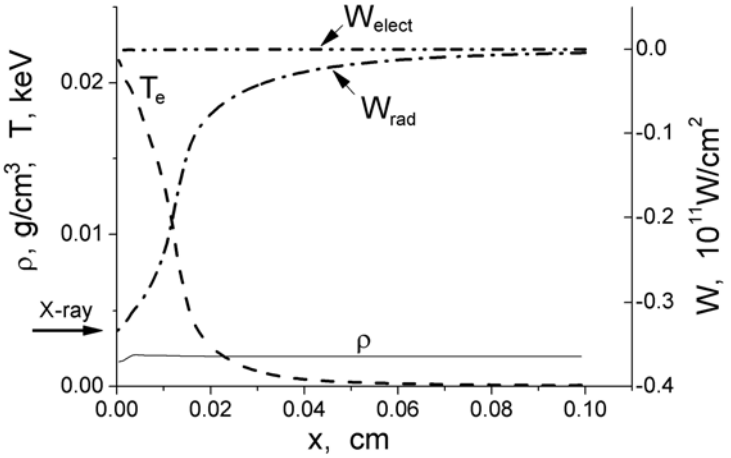

Fig. 4. The density, electron-temperature, and radiation-temperature profiles and fluxes of electron and radiation thermal conductivities at time of 1 ns. A plasma homogeneous layer with initial density 3 mg/cm^3 and thickness 1000 μm was irradiated by a thermal source with Planck radiation temperature 25 eV from the left boundary $x = 0$.

The thickness of the plasma layer is 1000 μm, and the initial density is 3 mg/cm^3. On the left immobile boundary at $x_0 = 0$ μm, the heating flux is constant and equals $W_{\rm Pl} = \sigma T_{\rm Pl}^4$. With time the temperature at the boundary rises and reaches a value of 25 eV, and the radiation wave covers an increasingly larger mass of the plane-layer material. A density profile forms at the radiation wavefront. With decrease in the initial density, the perturbation of the density profile under the action of the radiation wave becomes smaller. Thus, at an initial density lower than $\rho_0 = 2$ mg/cm^3 and under similar conditions, the deformation of the density profile is ∼10%, and at $\rho_0 = 3$ mg/cm^3 it is ∼70%.

The density ρ, electron-temperature T_e, and radiation-temperature T_r profiles and fluxes of electron $W_{\rm elect}$ and radiative $W_{\rm rad}$ thermal conductivities at time of 1 ns are given in Fig. 4. The electron thermal conductivity flux is negligibly small compared to the radiative thermal conductivity flux. Upon termination of the action of the external radiation source, the energy continues to be transferred by the flux of radiative thermal conductivity from the heated region to the cold one. The temperature of the heated region drops. For the speed of the radiation wave propagation under the action of the external radiation to be experimentally registered, the size of the layer and duration of the external-source pulse should be matched so that there is an unambiguous correspondence between the external source and the radiation wave.

Of special interest is the zone of low temperature (result of our calculations gives a "tongue" with temperature of 1–2 eV) with respect to the background temperature before the radiation wavefront (Figs. 3 and 4). It is determined by the occurrence of a hard X-ray radiation in the external heating spectral flux. The diffused profile of the radiation wavefront is also determined by the spectral composition of heating radiation. Let us discuss which elements of the spectral radiation flux are responsible for the heat-up dynamics of the plasma plane layer.

The behavior of the absorption coefficients determines the character of heating of the plasma layer by an external source. Figures 5–7 present dependences of the absorption coefficients and radiation fluxes on quantum energies in the plasma with the hydrodynamic profiles shown in Figs. 3 and 4. The absorption coefficient depends on the quantum energy and has a complex structure due to the large number of bound–bound and free–bound transitions (Fig. 5 a). At a time of 5 ns, in the spectral interval significant for the energy transfer ($h\nu < 300$ eV), the optical thickness of the plasma heated by the radiation wave is $\tau_{h\nu=50\ eV} = \chi'_{h\nu=50\ eV} \cdot \Delta r = 1.3$ for quantum energies $h\nu \sim 50$ eV, $\tau_{h\nu=75\ eV} = 34$ for $h\nu \sim 75$ eV, and $\tau_{h\nu=150\ eV} = 0.5$ for quanta $h\nu \sim 150$ eV, which is due to the particular features in the behavior of the absorption coefficient in the given range of temperatures and densities. Here, χ' is the absorption coefficient corrected for induced emission and taking into account free–free, free–bound, and bound–bound transitions. The optical thickness of this region for the Rosseland path length is ∼10. Thus, hard X-ray radiation (in this case, > 100 eV) can penetrate into the plasma much more deeply than the main flux of thermal radiation.

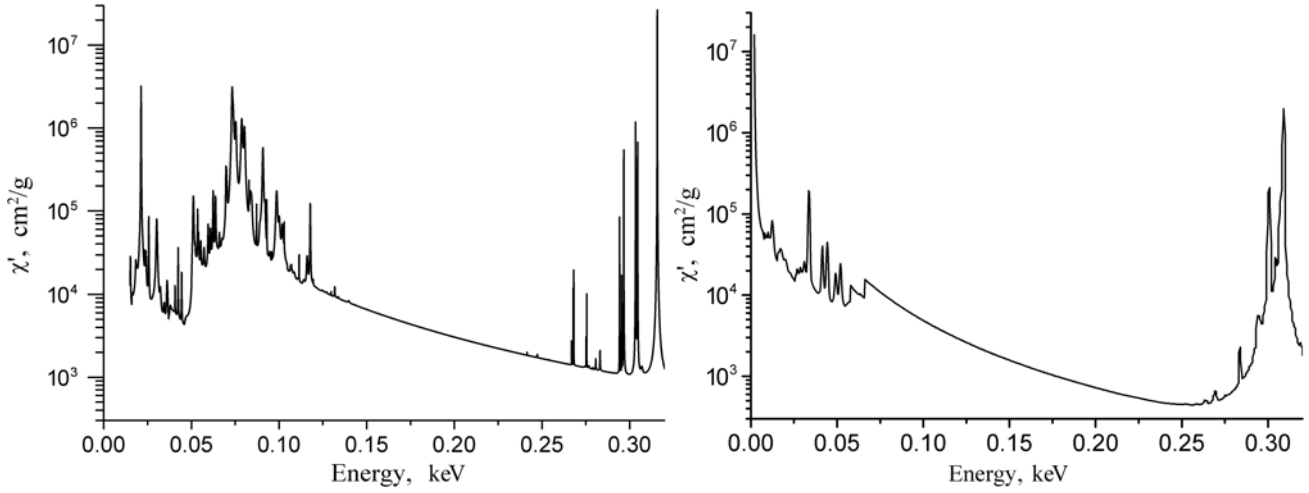

Fig. 5. The TAC absorption coefficient (left) and the CH absorption coefficient (right) at temperature 20 eV and density 3 mg/cm^3.

The density and temperature profiles are formed under the action of radiation waves propagating in the plasma. Figure 6 presents the spatial cross-sections of spectra of the radiation fluxes in a plane TAC plasma layer at time 5 ns. The flux of external radiation absorbed by the plasma is smaller than the heating spectral Planck radiation incident on the plasma because, already at time 1 ns, a layer of hot plasma is formed (Figs. 3 and 4). This layer is the source of intrinsic radiation. The thickness and temperature of this layer increase with time. The heated TAC layer radiates energy both into the plasma and towards the external source of radiation. As a consequence, an interesting result is observed — the radiation flux absorbed by the plasma has the spectra presented in Fig. 6 (curve 2) and does not coincide with the incident flux (solid bold curve 1). The gap in the spectral radiation flux at ∼70–100 eV is due

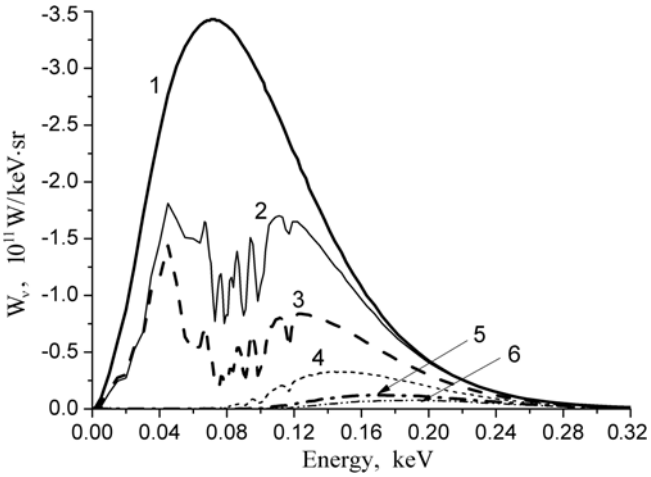

Fig. 6. Spectra of the radiation fluxes propagating through the plasma plane layer at time 5 ns. Incident heating spectral Planck flux of radiation corresponding to temperature 25 eV (curve 1), part of the external flux absorbed by the plasma (curve 2). Spectral fluxes of radiation at the spatial cross sections at $x =$ 300 μm (curve 3), 400 μm (curve 3), 500 μm (curve 3), and 650 μm (curve 3), i.e., those that passed the plasma layer of a given thickness.

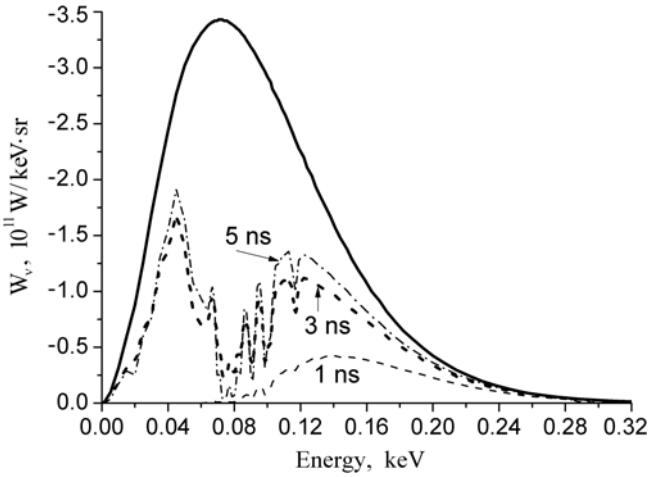

Fig. 7. Spectra of the radiation fluxes propagating through the plasma at the spatial cross-section $x =$ 200 μm and times $t = 1$, 3, and 5 ns. Incident heating spectral Planck flux of radiation corresponding to temperature 25 eV is shown by solid curve. A homogenous layer of the TAC plasma with initial density 3 mg/cm^3 and thickness 1000 μm was irradiated by a thermal source with Planck radiation temperature 25 eV for 10 ns from the left-hand-side boundary, $x = 0$.

to the absorption lines in oxygen present in TAC ($C_{12}H_{16}O_8$). With time the flux reradiated towards the incident external radiation increases, and the flux absorbed by the plasma decreases.

Figure 7 shows the spectra of the radiation fluxes propagating through the plasma at the spatial cross-section $x = 200$ μm and times $t = 1$, 3, and 5 ns. At time $t = 3$ ns, the radiation wave reaches the coordinate $x = 200$ μm. At subsequent times (including 5 ns), the radiation flux transferred by the radiation wave to the layer though this surface remains constant. With account for the temporal delay, the same can be said about the radiation wave propagating through any spatial cross-section of a plasma layer. A substantial feature of the hydrodynamic profile formation is the speed with which quanta of various energies enter a matter. The quanta determine the size, thickness, and exact shape of the radiation heat wavefront. It is seen in Fig. 3 that the temperature in the layer heated by an external radiation drops to the background temperature not as a jump and has a gradual smooth low-temperature front. The radiation wavefront penetrates to a great depth comparable with the full size of the heated plasma, and in the region of the radiation wavefront the plasma is heated up to a relatively low temperature, in this case ~1 eV. Different photons are responsible for the wavefront propagation at different times. The $x - t$ temperature origination diagram for 10 and 1 eV is shown in Fig. 8. To temperature 1 eV, the plasma is heated by a hard segment of the spectrum by photons with energies within the range of 100–300 eV, for which $h\nu/kT \sim 4 - 10$. The theory of radiation wave propagation predicts a low temperature before the wavefront but, as hard X-ray radiation penetrates here, the temperature in this region rises to 1 eV. This effect can be important in compression of thermonuclear-fusion targets, since an increase in temperature before the shockwave front prevents compression of the material.

Thus, there exists a broad penetrating zone on the temperature profile before the radiation wavefront (Figs. 3 and 4), which forms due to the occurrence of hard photons with spectral energies of $h\nu > 100$ eV

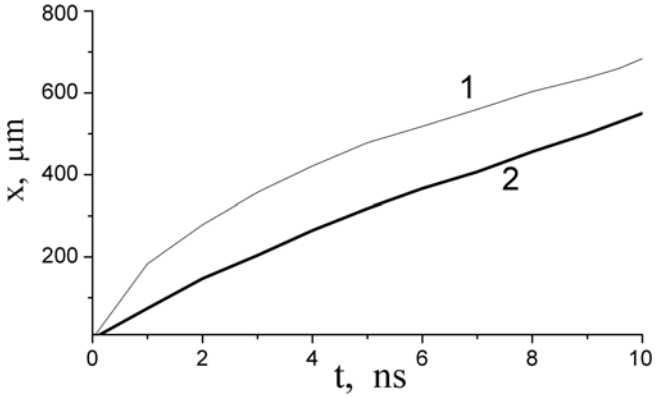

Fig. 8. The coordinate of the temperature front at a level of 1 eV (curve 1) and 10 eV (curve 2) as a function of time upon the action of an incident Planck flux of radiation, corresponding to a temperature 25 eV on a plane layer of the TAC plasma.

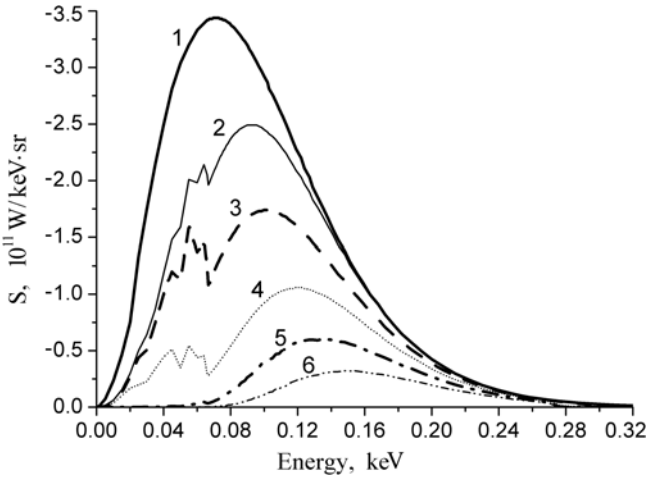

Fig. 9. Spectra of the radiation fluxes propagating through a plane layer of the CH plasma with initial density 3 mg/cm^3 at time 5 ns. The incident heating spectral Planck flux of radiation corresponding to a temperature of 25 eV (curve 1), a part of an external flux absorbed by the plasma (curve 2), and spectra of the radiation fluxes at the spatial cross-sections $x =$ 300 μm (curve 3), 400 μm (curve 4), 500 μm (curve 5), and 650 μm (curve 6).

in the initial spectrum (Figs. 6 and 7).

In Figs 5, 6, and 9, we present an example of the effect of optical constants on the plasma hydrodynamic characteristics. Consider the TAC and CH optical constants for temperatures up to 50 eV and densities 1–3 mg/cm^3. The TAC contains 44% oxygen by mass and 50% carbon. CH is 90% carbon. The presence of oxygen in the TAC ($C_{12}H_{16}O_8$) leads, first, to an increase in the absorption coefficient in the continuous spectrum, and second, to the emergence of absorption lines at quantum energies within the range of ∼70–100 eV due to transitions in the L-envelope of oxygen in the TAC. These lines emerge at temperatures above ∼10 eV. The nonequilibrium radiation heating the plasma has effective temperatures 20–40 eV, and this spectral range plays a significant role in the energy transfer. The results of numerical modeling depend nonlinearly on the optical coefficients used. At temperatures higher than 10 eV and density 2 mg/cm^3, the Rosseland path length for CH is greater than for TAC. Thus, at $T = 40$ eV for TAC $l'_{\text{Ross}} = 3.65$ cm, and for CH it is $l'_{\text{Ross}} = 16.6$ cm. This means that, upon the action of the same heating source on the plasma, absorption in TAC occurs in a smaller volume than in CH. Herewith, the temperature of the heated region in TAC is higher than that in CH.

In Fig. 9, we present the spectra of the radiation fluxes propagating through a plane layer of the CH plasma with initial density 3 mg/cm^3 at time 5 ns. The heating spectral Planck radiation flux incident on the plasma is also consistent with the temperature of 25 eV (compare Fig. 6). The energy absorbed by the CH plasma proves to be greater than that in the TAC case (curves 2 on Figs. 6 and 8) because the TAC plasma reradiates the absorbed energy towards the incident flux more efficiently than the CH plasma. At the same time, the external radiation flux penetrates into deeper layers of the CH plasma than in the TAC.

In Fig. 2, we present the coordinate of the radiation wavefront as a function of time for incident radiation fluxes corresponding to the Planck temperatures 15, 20, and 25 eV and duration 10 ns for various initial densities of the TAC layer of 1, 2, and 3 mg/cm^3. The radiation wave propagation speeds obtained as a result of numerical modeling are smaller than the speeds calculated by self-similar solution (7) [2]. As we have shown above, this is due to the fact that the self-similar solution does not take into account the reradiation of plasma towards the incident external source. In fact, the plasma is heated by a smaller thermal flux than the incident one. In addition, the self-similar solution does not take into account the motion of the plasma. The radiation wave propagates not along a cold matter but along the TAC preheated by hard quanta of external radiation.

4. Comparison with the Experiments

In the experiments [20, 21], a plane layer of low-density polystyrene foam (density 2 mg/cm^3 and thickness 800–1000 μm) was heated by a soft X ray radiation with effective Planck temperature of 15–40 eV. The experimental setup is described in [21]; here we only briefly communicate some experimental results. The registered passed radiation was 10–25% of the heating radiation energy incident on a layer.

To simulate these experiments, a series of calculations was performed, in which we varied the external radiation flux incident on the plasma layer $T_{\rm Pl} = 15-40$ eV, duration of the external pulse $\tau_{\rm Pl} = 5-10$ ns, thickness of the plasma layer $\Delta = 700-2000$ μm, and initial density of the plasma layer $\rho_0 = 1-3$ mg/cm^3. The calculations were made for polystyrene targets of various compositions: CH and $C_{12}H_{16}O_8$ (TAC).

Table 2 presents some results of the numerical modeling of those experiments.

A plane layer of plasma is heated by an external radiation flux $W_{\rm Pl}$ of temperature $T_{\rm Pl}$, duration $\tau_{\rm Pl} = 10$ ns, plasma layer thickness $\Delta = 800$ μm, and initial density of the plasma layer $\rho_0 = 2$ mg/cm^3. The composition of the heated target is given in column 4 of Table 2. The last column shows the ratio of the energy that passed through the layer to that incident on the layer.

Table 2. Results of the Numerical Modeling.

No	$T_{\rm Pl}$, eV	$W_{\rm Pl}$, 10^{11} W/cm^2	Material of target	$E_{\rm pass}/E_{\rm rad}$
1	15	0.0516	TAC	0.001
2	20	0.163	TAC	0.01
3	25	0.402	TAC	0.08
4	27	0.542	TAC	0.20
5	30	0.83	TAC	0.36
6	15	0.0516	CH	0.005
7	20	0.163	CH	0.03
8	25	0.402	CH	0.21
9	27	0.542	CH	0.32
10	30	0.83	CH	0.47

Due to the particular features in the behavior of the absorption coefficient, with the same modeling parameters the energy of radiation that passed through the CH is greater than in the TAC. In Fig. 10, we show an example of comparing the experimental data for the passage of a spectral radiation flux incident on a plane layer of the TAC plasma (thickness 800 μm and density 2 mg/cm^3) with the results of numerical modeling [21]. The heating spectrum of X ray radiation is given in the same figure. The energy and spectra of the radiation flux passing through a layer of the TAC is satisfactorily consistent with the experimental results.

5. Conclusions

We considered the propagation of radiation waves in the plasma of a porous low-density material upon the action of an external source of X-ray radiation having the Planck spectrum with $T_{\mathrm{Pl}} = 20 - 40$ eV. As a result, a plasma layer with relatively homogeneous spatial and temporal density and temperature profiles is formed. Numerical modeling shows that the speed of the radiation-wave propagation is lower than in classical theory [1,2]. This is due to the fact that the radiation flux absorbed by the plasma is smaller than the incident flux due to the losses for reradiation towards the heating flux.

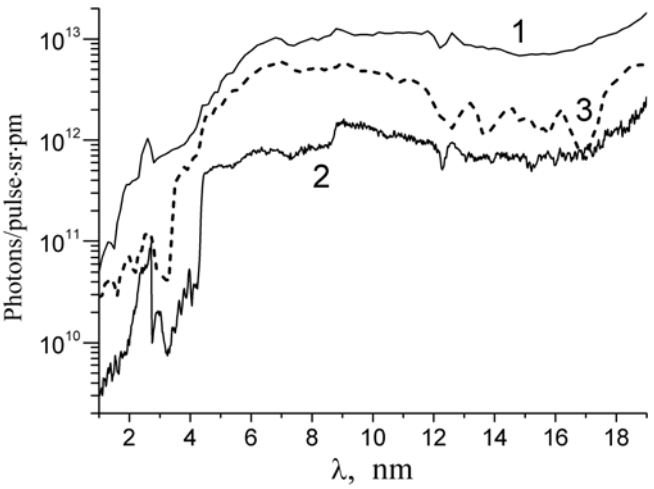

Fig. 10. Plasma-heating X-ray radiation spectrum (curve 1), spectrum of the radiation flux passing through the TAC layer (curve 2) registered in the experiment [21], and the results of the numerical modeling of the experiment (curve 3).

The structure of the wavefront (its curvature and speed of propagation) depends on the optical thickness and thickness of the plasma. The role of hydrodynamic processes in the formation of the plasma rises with increase in the material density because the speed of the radiation wave decreases with increase in the material density. The spatial inhomogeneity decreases as the density decreases. Figure 3 demonstrates the spatial inhomogeneity (corresponding to a higher density of 3 mg/cm^3) reaching 70%, and at a density of 2 mg/cm^3 it reaches 10%.

The form of the wavefront differs from the classical form by the low-temperature front penetrating deep into the plasma. An important role in this respect is played by hard quanta occurring in the incident flux ($h\nu > 100$ eV), which penetrates to a greater depth as compared with the classical wavefront and gives rise to a definite structure. This behavior is observed in Fig. 3.

The physical-mathematical model used for numerical modeling is adequate for the experimental conditions. The integral and spectral characteristics of the outgoing plasma radiation obtained as a result of numerical modeling are satisfactorily consistent with the experimental data.

Acknowledgments

This work was supported by Program No. 2 "Matter at High Energy Densities" (2012–2013) of the Presidium of the Russian Academy of Sciences and the Russian Foundation for Basic Research under Project No. 11-02-01305.

References

1. R. E. Marshak, *Phys. Fluids*, **1**, 24 (1958).
2. Y. B. Zel'dovich and Y. P. Raizer, *Physics of Shock Waves and High-Temperature Hydrodynamic Phenomena*, Academic Press, New York (1966).

3. J. I. Castor, *Radiation Hydrodynamics*, Cambridge University Press (2007).
4. J. H. Hammer and M. D. Rosen, *Phys. Plasmas*, **10**, 1829 (2003).
5. R. Sigel, G. D. Tsakiris, F. Lavarenne, et al., *Phys. Rev. Lett.*, **65**, 587 (1990).
6. J. M. Yang, Y. Xu, Y. N. Ding, et al., *Chin. Phys. Lett.*, **20**, 90 (2003).
7. J. M. Yang, Y. Xu, Y. N. Ding, et al., *Chin. Phys. Lett.*, **20**, 256 (2003).
8. G. A. Vergunova and V. B. Rozanov, *Sov. J Quantum Electron.*, **22**, 239 (1992).
9. M. D. Rosen and J. H. Hammer, *Phys. Rev. E*, **72**, 056403 (2005).
10. N. G. Borisenko, Yu. A. Merkuliev, and A. I. Gromov, *J. Moscow Phys. Soc.*, **4**, 47 (1994).
11. A. M. Khalenkov, N. G. Borisenko, V. N. Kondrashov, et al., *Laser Part. Beams*, **24**, 283 (2006).
12. J. Falconer, W. Nazarov, and C. J. Horsfield, *J. Vac. Sci. Technol.*, **A13**, 1941 (1995).
13. P. E. Young, M. D. Rosen, J. H. Hammer, et al., *Phys. Rev. Lett.*, **101**, 035001 (2008).
14. M. Lebedev, K. Dyabilin, K. Eidmann, et al., *Phys. Lett. A*, **240**, 73 (1998).
15. Shaoen Jiang, Yan Xu, Yongkun Ding, Dongxian Lai, et al., *Sci. China Ser. G: Phys. Mech. Astron.*, **48**, 549 (2005).
16. C. A. Back, J. D. Bauer, J. H. Hammer, et al., *Phys. Plasmas*, **7**, 2126 (2000).
17. J. Limpough, N. N. Demchenko, S. Yu. Guskov, et al., *Plasma Phys. Control. Fus.*, **46**, 1831 (2004);
18. V. Rozanov, D. Barishpoltsev, G. Vergunova, et al., *J. Phys. Conf. Ser.*, **112**, 022010 (2008).
19. V. Rozanov, E. Aristova, D. Barishpoltsev, et al., "Analysis of the energy transfer in low-density structured foam-like targets in experiments on the LIL facility," *Proceedings of the XXX ECLIM (European Conference on Laser Interaction with Matter, Darmstadt, Germany, August 31 – September 5, 2008)*, Technische Universität Darmstadt, Darmstadt, Germany (2009), p. 49.
20. D. H. H. Hoffmann, A. Blazevic, P. Ni, et al., *Laser Part. Beams*, **23**, 47 (2005).
21. O. N. Rosmej, V. Bagnout, U. Eisenbarth, et al., *Nucl. Instrum. Methods A*, **653**, 52 (2011).
22. G. A. Vergunova, S. Yu. Gus'kov, O. N. Rosmej, and V. B. Rozanov, *J. Russ. Laser Res.*, **31**, 59 (2010).
23. A. F. Nikiforov, V. G. Novikov, and V. B. Uvarov, *Quantum Statistical Models of High-Temperature Plasma* [in Russian], Fizmatlit, Moscow (2000).
24. N. Yu. Orlov, *Laser Part. Beams*, **15**, 627 (1997).
25. E. Ivanov, V. Rozanov, and G. Vergunova, *SPIE Proc.*, **4424**, 308 (2001).
26. G. A. Vergunova, V. B. Rozanov, O. B. Denisov, et al., *Plasma Phys. Rep.*, **39**, 755 (2013).